IEEE Access
Multidisciplinary | Rapid Review | Open Access Journal

Received 29 June 2022, accepted 19 July 2022, date of publication 28 July 2022, date of current version 4 August 2022.

*Digital Object Identifier 10.1109/ACCESS.2022.3194525*

RESEARCH ARTICLE

# Hermite Transform Based Algorithm for Detection and Classification of High Impedance Faults

**DANIEL GUILLEN[1], (Member, IEEE), JIMENA OLVERES[2], VICENTE TORRES-GARCÍA[2], (Senior Member, IEEE), AND BORIS ESCALANTE-RAMÍREZ[2]**

[1]Escuela de Ingeniería y Ciencias, Tecnologico de Monterrey, Monterrey 64849, Mexico
[2]Facultad de Ingeniería, Coyoacán, Universidad Nacional Autónoma de México, Mexico City 04510, Mexico

Corresponding author: Jimena Olveres (jolveres@cecav.unam.mx)

This work was supported in part by the Universidad Nacional Autónoma de México by means of the Programa de Apoyo a Proyectos de Investigación e Innovación Tecnológica (PAPIIT), grant TA101121 and grant IV100420.

**ABSTRACT** This work proposes a new algorithm to classify high impedance faults (HIFs) in distribution systems. HIFs can be represented by small current magnitudes with non-linear variations, which complicate their detection in distribution grids. The proposed method uses the Hermite transform (HT) as a signal processing technique that offers several advantages, one of the more important being the ability to analyze the signal at multiple resolution levels and at different frequency bands thanks to their filter functions based on Gaussian derivatives. The Hermite coefficients are used to extract signal features that allow efficient identification of the transient behaviour related to HIFs and other typical faults. In this sense, a multichannel approach based on the Hermite transform is proposed to classify different types of faults and HIFs. This analysis is carried out in a distribution network considering photovoltaic (PV) systems considering three different classifiers, which are also used to compare our results with the discrete wavelet transform (DWT) as signal decomposition model; the comparison suggests that our proposal presents better performance discriminating HIFs from typical faults.

**INDEX TERMS** Classification, distribution grids, fault detection, Hermite transform, high impedance faults, multiresolution analysis, photovoltaic systems.

## NOMENCLATURE

| | |
|---|---|
| $H_n$ | Hermite polynomials. |
| $L_n$ | Hermite-expansion coefficients. |
| $D_n$ | Filter functions. |
| $G(x)$ | Gaussian window. |
| $i(x)$ | Electrical signal. |
| $v$ | Arc voltage. |
| $i$ | Arc current. |
| $\tau$ | Time constant. |
| $g(t)$ | Arc conductance. |
| $P(v, i)$ | Arc power in steady-state. |
| $I_a, I_b, I_c$ | Line currents. |
| $I_{HTa}, I_{HTb}, I_{HTc}$ | High-frequency components. |
| $F_1$ | Standard deviation. |
| $F_2$ | Average absolute magnitude. |
| $F_3$ | Average energy. |
| $F_4$ | Kurtosis index. |

The associate editor coordinating the review of this manuscript and approving it for publication was Inam Nutkani.

## I. INTRODUCTION

The aim of a distribution system (DS) is to supply energy to all demanding customers. Grid congestion and distances associated to power distribution expose the grid to critical conditions such as faults and abnormal scenarios, which may affect the power quality and the system reliability. In this context, the protection systems must be reliable to detect faults as fast as possible to avoid large interruptions of load. One of the more important issues of distribution grids is the protection against short circuits that produce high current magnitudes resulting from "low impedance fault (LIFs)". However, in some cases, the fault may present small current

magnitudes originated by ''high impedance faults (HIFs)'', which are characterized by a nonlinear behavior [1], [2]. Therefore, the correct discrimination between LIFs and HIFs has become an essential subject of interest because HIFs present complex transient behaviours that complicate their detection. A HIF occurs when an overhead conductor makes contact with any object that hosts a path to ground. Due to the small current magnitudes and the nonlinearity of the phenomenon, HIFs may not be detected by conventional overcurrent protections [3]. The resulting resistance during a HIF limits the fault current but the current magnitude is below the detectable limit (pick-up current) by a conventional overcurrent protection. Fault current magnitudes are generally smaller than 75 amperes, particularly in 12.47 kV feeders, depending also on the contact surface [4]. For example, typical fault current levels at a bus of distribution substations are around 5–6 kA, whereas at the end of the feeder the fault currents can drop to 1.5 kA and the load currents range is between 300-500 A. So, for a conventional ground fault relay set to detect faults between 200–300 A, a HIF that produces magnitudes smaller that 75 A will be undetectable. As a consequence, the problem of HIF detection has been tackled form a signal processing perspective, associating transient characterization to the electric arc phenomenon. The arc phenomenon is non-linear, asymmetric, and unpredictable, which makes the detection of HIFs in distribution grids a complex task. Therefore several recent studies aim at characterizing the patterns of voltage and current signals related to HIFs.

In general, the analysis of HIFs can be carried out in time, frequency, or time-frequency domains in which feature characterization is developed achieved by advanced signal processing and artificial intelligence techniques. For instance, in [5] a methodology based on the harmonic content has been implemented, in which the detection uses odd and even harmonics of the current signal to distinguish HIFs from other transient phenomena. In a similar approach [6] evaluates the even harmonics in the voltage waveform by using smart meters (SMs). In [7] the incorporation of inter-harmonic components superimposed onto the current of conventional protections such as automatic recloser and sectionalizer is analyzed, demonstrating that this method facilitates the detection due to the variations found in the inter-harmonics. Following the same basis of inter-harmonics, the complex nature of HIFs has motivated the development of new proposals using multiresolution approaches; for instance, [8] combines two techniques such as maximum overlap discrete wavelet packet transform (MODWPT) and empirical mode decomposition (EMD), demonstrating effective outcomes during the detection and classification of HIFs.

Due to the nonlinear behaviour and the intermittency of the electric arc, the current waveforms present asymmetries that can be detected by multiresolution techniques. For example, in [9], [10] a simplified version of the discrete wavelet transform (DWT) uses the energy of the wavelet coefficients to detect HIFs within a sliding window of size equal to the fundamental period. In a similar way, [11] introdues a DWT-based method that monitors the high- and low-frequency components of voltage through the system. Another way to deal with HIFs in distribution networks is based on power spectral density (PSD) estimation from a multiresolution analysis by using the DWT [12], in which the detection and classification process is carried out in a radial distribution system. In [13] a DWT-based ensemble Random Subspace (RS) classifier is proposed for discriminating HIFs in distribution grids with a photovoltaic system, using three classifiers, namely K-nearest neighbour (KNN), logistic regression (LR), and random tree (RT).

Other techniques such as mathematical morphology, empirical mode decomposition (EMD), and morphological gradient have been employed for HIFs detection and classification [14]–[17]. In [15], a multistage morphological-based fault detector is proposed to cope with HIFs in distribution systems by extracting the nonlinear features of HIFs. In a different approach, the EMD-based method proposed in [16] uses voltage signals to identify the predominant harmonic components, and the classification is performed by applying an artificial neural network (ANN). In the same context, in [18] a multilayer perceptron (MLP) is proposed. In this case the classification method is based on higher-order statistics (HOS), which is also combined with Fisher's discrimination ratio to extract specific patterns associated with the HIFs. The multi-resolution morphological gradient (MMG) method has also proved to be an effective tool for discriminating HIFs from other transient phenomena [17]. This method analyses the fault currents in order to extract the main features that are used as inputs to a multi-layer perceptron neural network. In the same context, a classifier named Boosted Decision Trees (BDT) has been applied in HIFs [19]; the proposed method employs the high-frequency components and was tested with a real data set comprising a large number of experiments that were also assessed in the presence of noise. Another approach based on time-frequency analysis and a support vector machine (SVM) classifier was proposed by [20]. A similar application of SVM is reported in [21], which is combined with Principal Component Analysis (PCA) to cope with the detection and classification of HIFs.

Other techniques based on time-domain analysis have been recently introduced. For instance, in [22] the superimposed high-frequency components of voltages and currents are analyzed using the moving sum of one cycle of the fundamental frequency. Moreover, a time-domain approach focusing on fault location based on a linear least square-based estimator is also applied in [23]. In general, the limitations and advantages of all different applied methods depend on the selection of signal processing techniques and feature extraction processes. This paper proposes a new method based on the Hermite transform (HT) as a tool to extract relevant features that allow HIF discrimination form other faults.

The main contribution of this work is the development of a new method able to discriminate typical faults from HIFs in distribution networks by including distributed generation

based on photovoltaic (PV) generation. This paper considers a HIF obtained from a bare conductor in touch with dry grass in a 13.8 kV distribution grid. The method employs a multiresolution and multifrequency scheme based on the HT. The electrical signal is analysed by means of the basis filter functions of the HT which extract relevant features that are used to discriminate and classify failures. The classification process is mainly developed using four different characteristics defined by the high-frequency components. The proposed scheme is assessed by employing three different classifiers KNN, SVM, and NN. In addition, results are compared with those obtained by an approach based on the DWT.

## II. HIGH IMPEDANCE FAULTS MODELLING AND ANALYSIS

### A. HERMITE TRANSFORM

The Hermite transform is an efficient signal representation model that has proven to be useful to analyse electrical signals (voltage and current signals). The main transient components of an electrical signal $i(x)$ can be extracted by expanding the signal into the Hermite polynomials [24]. The decomposition of the signal $i(x)$ is locally carried out by sliding a Gaussian window $G(x-kT)$ at overlapping positions $kT$, which can be expressed in the time domain as follows:

$$G\left(x-kT\right)\left[i(x)-\sum_{n=0}^{\infty}L_n\left(kT\right)H_n\left(x-kT\right)\right]=0 \quad (1)$$

where $H_n(x)$ corresponds to the Hermite polynomials, whereas $L_n(kT)$ stands for the expansion coefficients.

The Hermite polynomials $H_n(x)$ build an orthogonal basis with respect to a Gaussian window. Therefore, the expansion coefficients can be obtained with [24]:

$$L_n\left(kT\right)=\int_{-\infty}^{\infty}i\left(x\right)H_n\left(x-kT\right)G^2\left(x-kT\right)dx \quad (2)$$

Expression (2) shows the polynomial expansion coefficients $L_n(kT)$ of a signal $i(x)$; in fact, the coefficients $L_n(kT)$ can be computed through a convolution between the filter functions $D_n(x)$ and the studied signal $i(x)$. Notice that the process is followed by a subsampling process at multiple positions of $T$, and the filter functions $D_n(x)$ are defined by:

$$D_n\left(x\right)=H_n\left(-x\right)G^2\left(-x\right) \quad (3)$$

It can be shown that the filter function of order $n$ corresponds to the $n^{th}$ derivative of a Gaussian function, therefore filter functions $n$ can also be represented by [24]:

$$D_n\left(x\right)=\frac{1}{\sqrt{2^n n!}}\frac{d^n}{d\left(\frac{x}{\sigma}\right)^n}\left[\frac{1}{\sigma\sqrt{\pi}}e^{\left(-\frac{x^2}{\sigma^2}\right)}\right] \quad (4)$$

The subsampling period $T$ is a free parameter with the only restriction that the adjacent Gaussian windows must overlap.

The HT presents several advantages over other decomposition schemes. One of the most relevant advantages is its optimal resolution in time-frequency based on the uncertainty principle due to the Gaussian window of analysis. Moreover, filtering with Gaussian functions guarantees no spurious artifacts in the resulting analyzed signals, according to the scale space theory. Additionally, the analysis filters (Gaussian derivatives) have proven to be efficient feature detectors. The multiscale analysis of the studied signal can be performed by systematically increasing the Gaussian window width; this process allows detecting any transient component (frequency components) at different time scales [25], [26].

### B. MODELLING OF HIGH IMPEDANCE FAULTS

HIFs in distribution grids are frequently composed of non-linear characteristics resulting from an electric arc and the contact surface, these are responsible for developing small current magnitudes, a non-linear dependency between voltages and currents, and asymmetric current waveforms. These characteristics can be used to develop HIF models. The behaviour of HIFs can be understood using a non-linear resistance, which facilitates the implementation to conduct simulations. In this work, a HIF model based on the arc conductivity is used, which is developed by a first-order differential equation [5].

$$\frac{d\left(\ln g(t)\right)}{dt}=\frac{1}{\tau}\left(\frac{vi}{P}-1\right) \quad (5)$$

where $v$ and $i$ represent the arc voltage and current, respectively; $g(t)$ is the arc conductance, $\tau(v, i)$ is the time constant, and $P(v, i)$ is the arc power in steady-state. Then, by taking $\tau$ as a constant and the steady-state power as $P = P_0 + v_0 i$, the solution to (5) can be obtained.

According to [5], the general equation to represent the arc conductance in the time domain is expressed by:

$$g(t)=G_0(1-e^{-t/\tau}) \quad (6)$$

where $g(t)$ is the time-varying conductance and $G_0$ is the steady-state conductance. It should be mentioned that the time varying resistance $r(t)$ can be obtained by the inverse of $g(t)$.

The parameters $G_0$ and $\tau$ reported in [5] are obtained from measurements using the least square method. For instance, if one has a voltage signal $v_f(t_k)$ and a current signal $i_f(t_k)$ corresponding to a real HIF, the arc conductance $g_f(t_k)$ can be computed by

$$g_f(t_k)=\sqrt{\frac{\sum_{i=-n}^{n}i_f^2(t_{k+i})}{\sum_{i=-n}^{n}v_f^2(t_{k+i})}} \quad (7)$$

where $n$ is the number of samples of one cycle of the fundamental frequency and the discrete-time instants are denoted by $t_1, t_2, \cdots, t_N$. Finally, to determine the arc parameters $S(G_0, \tau)$, the minimization process is defined by

$$S(G_0,\tau)=\sum_{k=1}^{N}[g(t_k)-g_f(t_k)]^2 \quad (8)$$

Due to the need to interface the non-linear conductance-resistance model with the standard models, in this work, the model is implemented with a non-linear resistance by using a

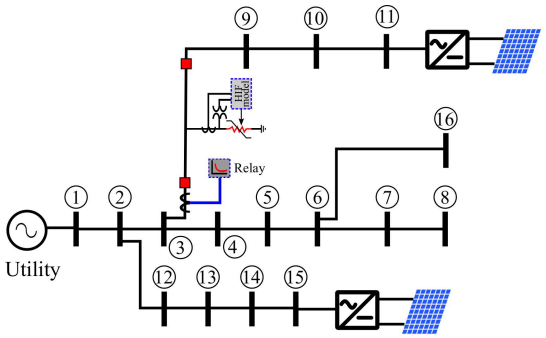


**FIGURE 1.** HIF model implemented in Matlab-Simulink.

block of a controlled current source through Matlab-Simulink software. Other HIF models can be found in [18].

### C. HIFs ANALYSIS BASED ON THE HERMITE TRANSFORM

Figure 1 shows a test system to cope with the signal processing of HIFs in active distribution networks. The sampling frequency used is 6.4 kHz for a fundamental frequency of 50 Hz. A HIF was simulated between buses 3 and 9 of the test systems. In this case, Fig. 2a) depicts the HIF current at the fault point along the fault period. In addition, the corresponding voltage-current (V-I) characteristics are shown in Fig. 2b). Finally, the line currents seen by the protection devices are represented in Fig. 2c). In this case, a current transformer (CT) with a ratio of 100:5 was employed. Due to the current magnitudes of HIFs, the CT will not experience the saturation phenomenon.

Figure 3 depicts the HT coefficients where plots correspond to different HT coefficients, which in turn represent different time-frequency levels of analysis of a typical HIF signal. HT coefficients are normalized in order to improve the sensitivity of high-frequency components of a HIF. HT coefficient calculation will be used to detect and classify HIFs in distribution as will be discussed later.

## III. CLASSIFICATION APPROACH FOR HIGH IMPEDANCE FAULTS

### A. FEATURE EXTRACTION

The effectiveness of any classifier to discriminate typical faults resulting from high impedance faults depends on the efficiency of the feature extraction process. Feature extraction of high impedance faults is not an easy task since current magnitudes may present small changes that can be interpreted as load variations [21]. As a consequence, HIFs require robust algorithms able to distinguish them from other fault types. One effective way to extract the most relevant characteristics of HIFs is commonly based on multiresolution approaches [19], [27]. In general, multiresolution analysis facilitates feature extraction because it provides information in time and frequency at different resolution levels. A suitable feature selection is therefore essential to improve classification performance.

In this work, feature extraction is performed through a Hermite transform-based approach that obtains the

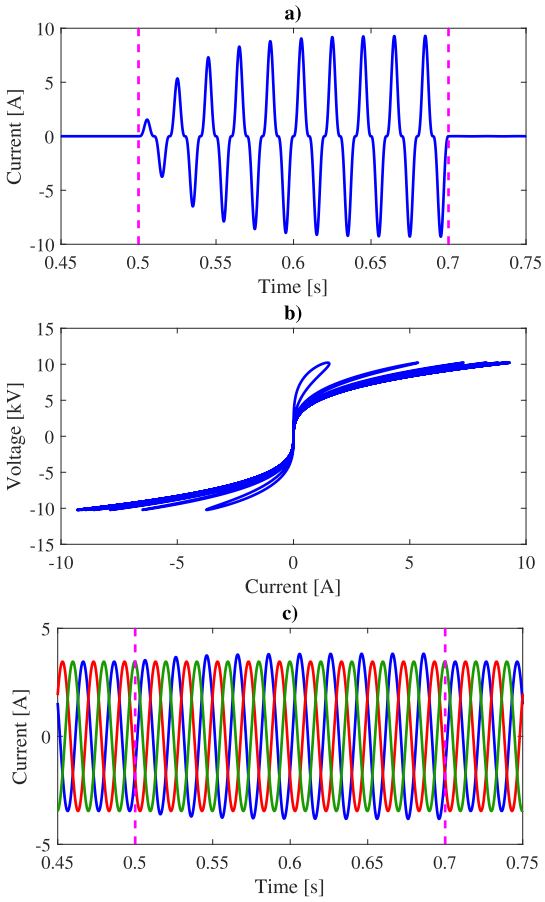


**FIGURE 2.** HIF in a distribution network: a) current, b) V-I characteristics, and c) line currents seen by the digital relay.

high-frequency components of the analysed signals by means of the HT coefficient calculation. The analysis employs different time-frequency resolution levels that allow identifying the most relevant transient characteristics, which are used to establish the feature extraction defined by statistical indexes. To avoid the problem of high dimensionality, a max-pooling process is carried out to reduce the transient information obtained by means of the HT coefficients at each resolution level. As argued before, classification performance relies on the feature selection process [19] and outcomes are highly dependant on the training process, that is, low performance scores in the training stage means that the features used are not good enough to separate classes. For example, to overcome the disadvantage of using features by trial and error, in [28], [29] the authors employ a matrix defined by eight features, some of them depending on statistical indices. In this case, we opted for only four features defined by:

$$F_1 = \sqrt{\frac{1}{N-1}\sum_{k=1}^{N}(y_k - \mu)} \tag{9}$$

$$F_2 = \frac{1}{N}\sum_{k=1}^{N}|y_k| \tag{10}$$

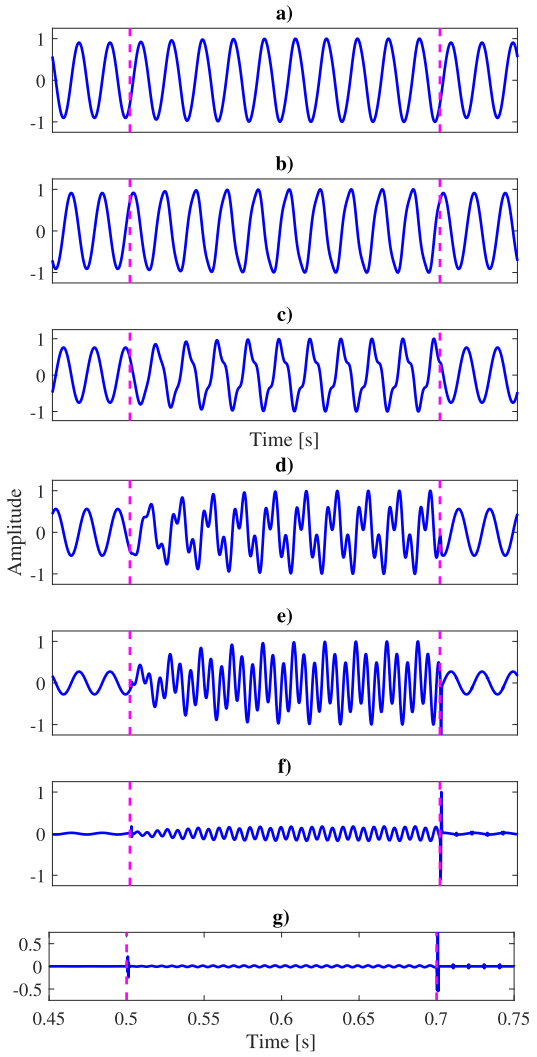


**FIGURE 3.** HT coefficients of a HIF signal: a) 0 order, b) 1st order, c) 2nd order, d) 3rd order, e) 4th order, f) 5th order, g) 6th order.

$$F_3 = \frac{1}{N}\sum_{k=1}^{N} y_k^2 \tag{11}$$

$$F_4 = \frac{(1/N)\sum_{k=1}^{N}(y_k - \mu)}{(1/N)\left(\sum_{k=1}^{N}(y_k - \mu)^2\right)^2} \tag{12}$$

where $N$ is the number of samples, $\mu$ represents the average value, $F_1$ corresponds to the standard deviation, $F_2$ is the average absolute magnitude, $F_3$ stands for the average energy, $F_4$ represents the Kurtosis index, and $y_k$ ($I_{HTa}$, $I_{HTb}$ and $I_{HTc}$) stores the most essential transient components (HT coefficients from 1st to 6th order) defined by the determinant of the matrix resulting from the max-pooling process.

### B. PROPOSED APPROACH

This proposal introduces a new method to detect and classify HIFs as well as typical faults in distribution systems. The proposed approach is summarized in Fig. 4, which consists of six stages. First, the electrical signals are measured on the protected line by employing current transformers (CTs). Next, all measured signals $I_{line}$ ($I_a$, $I_b$, and $I_c$) are processed by the HT to extract the high-frequency components. To this aim, the process consists of representing all transient frequency components at different resolution levels by computing the convolution between the measured signal and the Hermite filter functions. Therefore, each current signal $I_{line}$ will be represented by a matrix of $N$ samples and $L$ resolution levels $I_{HTC-line}$. In this work, the Gaussian derivatives from 1-st to 6-th are used according to the HT decomposition scheme. Then, to distinguish HIFs from typical faults, a max-pooling process with sliding window is carried out to reduce the transient information; for this purpose, it is suggested to use a number of resolution levels (or level of decomposition) multiple of three, this means that the matrix size employed for the max-pooling process will be $L \times L$, which is partitioned in four sub-matrices of $L/3 \times L/3$. The max-pooling is applied to each sub-matrix giving as a result a new matrix of $2 \times 2$, and this new matrix is used to compute its determinant in order to have only one value per analysed window. The determinant of the resulting matrix is computed so that the new signal $I_{HT-line}$ is represented by one dimension, that is, $N$ samples. This signal $I_{HT-line}$ will store all transient components used to the feature extraction. The feature extraction process will define the inputs of the classifier. Finally, the complete data set is divided to conduct the training and validation stages of classification to distinguish HIFs from typical faults.

For better understanding, Fig. 5 shows the stages of the proposed approach. The line currents are processed using the HT, where the HT coefficients are employed to extract the most essential high-frequency components. Notice that this proposal faithfully captures the transient information produced by HIFs in distribution systems. For example, Fig. 5a) depicts the line currents ($I_a$, $I_b$, and $I_c$) where small changes in the current magnitudes occur at $t = 0.5$ s. Based on the proposed method, the processing of the HT coefficients permits to identify the most relevant transient components, as pictured in Fig. 5b), both for the non-faulted phases ($I_{HTb}$ and $I_{HTc}$) and the faulted phase $I_{HTa}$. Finally, the extracted features are shown in Fig. 5c) which correspond to the faulted phase $I_a$ just after processing the HT coefficients stored in $I_{HTa}$.

### C. CLASSIFIERS

Classification of high impedance and typical faults was achieved with three different classifiers, namely: K-nearest neighbour (KNN), support vector machine (SVM) and artificial neural networks (ANNs).

#### 1) K-NEAREST NEIGHBOUR (KNN)

KNN is a supervised classifier based on a distance metric and $K$ number of neighbours defined by the user [30]. Given a set of training samples belonging to a number of different classes, a new sample is assigned to the class which most frequent K-nearest neighbours belong to. In addition, to overcome bias in the class prediction due to unbalanced data,

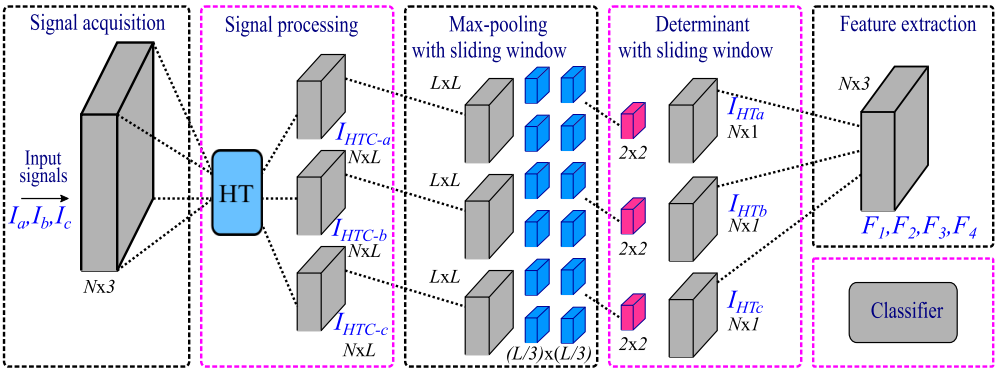


**FIGURE 4.** Schematic diagram of the proposed approach.

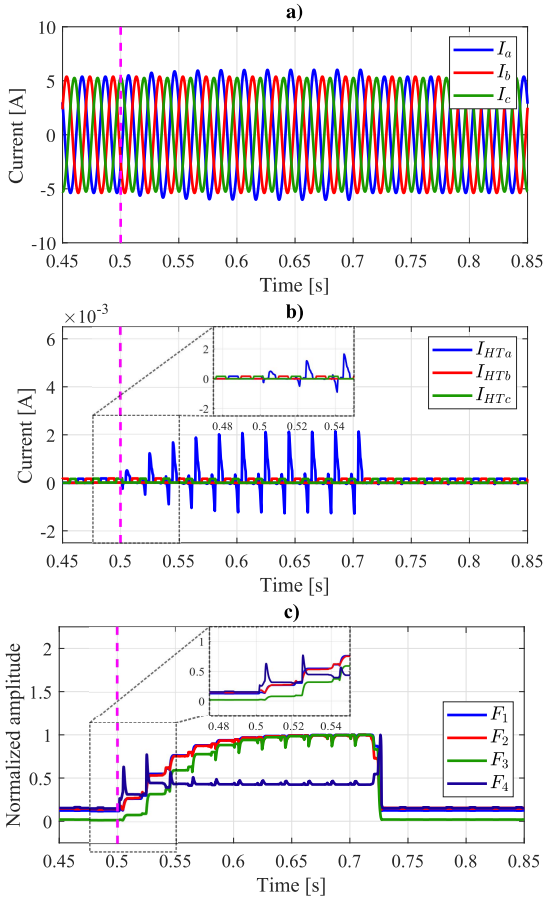


**FIGURE 5.** HIF simulated: a) line currents seen by the digital relay, b) transient components-based algorithm using HT, and c) features.

weight proportional to the inverse of the distance from the $K$ neighbours is assigned to each class. $K$ is an important tuning parameter and its choice affects computing time and classification performance. For this work, $K$ is 5 and the selected metric was Euclidean.

### 2) SUPPORT VECTOR MACHINE (SVM)

Support vector machine is a widely known algorithm for supervised learning. This classifier uses an objective function aiming at minimizing misclassification errors by maximizing

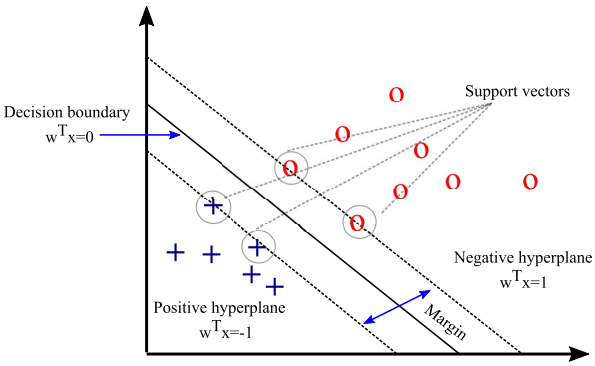


**FIGURE 6.** Support vector machine diagram.

the separation margin. It also separates classes by constructing an hyperplane in the high dimensional features as shown in Fig. 6.

For instance, in a two-class problem, the mapping consists of a two-stage dataset $(x_i y_i)_{i=0}^{N}$ with $N$ data points where $x_i$ is the training data, and $y_i$ is the corresponding class, which takes values of $+1$ and $-1$. In this sense, the margin is the distance between the separating hyperplane and the training samples that are closest to the hyperplane, these are also called support vectors. The hyperplane separates both categories, and its equation is:

$$w^T x_i + b = 0 \tag{13}$$

where $\omega$ represents the vector normal to the hyperplane, and $b$ is the bias parameter; both parameters determine the position of the hyperplane. In the training stage, the best values of these parameters are obtained such that they maximize the separation between both categories, obtaining the separation margin as $m = 2/\|m\|$. Therefore, the objective function will maximize the margin defined by the relation between $m$ (margin value) and $\omega$, that is, the solution allows obtaining these values, and the samples are classified correctly as [31]:

$$y^{(i)}(w_0 + w^T x^{(i)}) \geq 1, \forall_i \tag{14}$$

Finally, the classification is carried out by separating all negative samples on one side of the hyperplane (first class), and the positive samples on the other side of the hyperplane

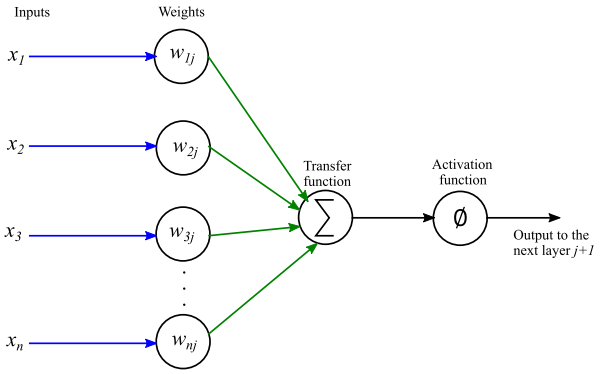


**FIGURE 7.** Single-layer neural network.

(second class). Additionally, SVMs can be converted into a multivalued classifier using a one to one method. In this work, a Gaussian radial basis function (RBF) kernel and a cross-validation procedure were used during during training.

#### 3) ARTIFICIAL NEURAL NETWORKS (ANNs)

ANN classifiers are widely used in machine learning and have proven to be powerful supervised learning algorithms because of their parallel processing, nonlinear mapping, and associative memory. Multilayer neural networks are able to produce robust diagnosis in different areas of electric power systems [32]. The method consists of a training stage,in which network weight parameters are tuned by means of back-propagation so that a cost function is minimized. Next equation shows the iterative process to update the weights through back-propagation.

$$\begin{aligned} w &:= w + \Delta w, \\ \Delta w &= -\eta \nabla J(\omega) \end{aligned} \tag{15}$$

where, $w$ represents the weights, which are updated by taking a step in the opposite direction of the gradient $\nabla I(\omega)$. Moreover, the gradient is multiplied by a factor known as the learning rate $\eta$.

In general, the learning rate balances the speed of the learning with the overshoot of the global minimum of the cost function, which is usually defined by the sum of square errors. A graphical basic architecture of a single-layer neural network is shown in Fig. 7. For a multilayer scheme, the output is connected to the next layer and so on. In this application, 10 layers are used and the activation function corresponds to the cross-entropy.

## IV. PRACTICAL IMPLEMENTATION ASPECTS

From a practical point of view, digital signals require discrete computation and the general overview of a practical implementation is shown in Fig. 8. For applications in distribution systems, the line currents $I_a, I_b, I_c$ of a specific protected distribution line are sampled by means of an analog-to-digital converter device. Once the signals are sampled, the discrete Hermite transform is calculated and two approaches can be followed according to [24]. The first

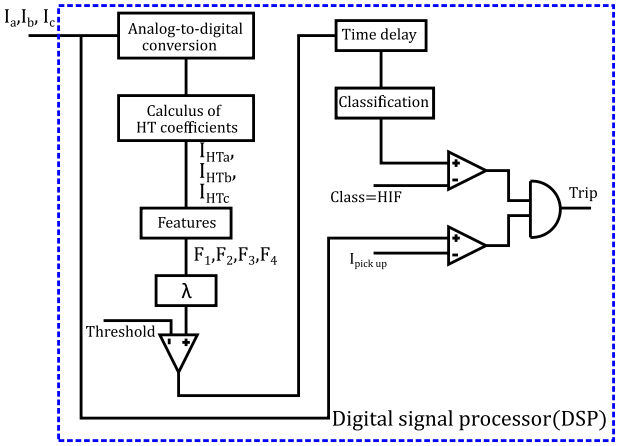


**FIGURE 8.** Logic of detection based on HT.

one consists of approximating the continuous filter functions by finite-support discrete filters; the second one uses a discrete polynomial expansion, that is, the continuous Hermite polynomials are approximated by discrete polynomials (Krawtchouk polynomials), which are orthogonal with respect to the binomial window function, which in turn approximates the Gaussian window. Both approaches achieve similar results, and the first one is chosen to calculate the HT coefficients of the studied signals. The spread of the approximated Gaussian function can be tuned to maximize detection of time-frequency features of the HIF signals. Each signal is analysed by expanding its transient information according to the HT, and the produced Hermite coefficients $L_n(kT)$ (or $I_{HTCa}, I_{HTCb}, I_{HTCc}$) are processed using a max-pooling process to reduce the transient information stored at each resolution level allowing us to find the most significant features. In this work, only four features are used to discriminate HIFs from typical faults by means of a classification stage. The full scheme of HIF detection can be implemented in a digital signal processor (DSP) summarized in Fig. 8.

## V. RESULTS AND DISCUSSIONS

### A. DISTRIBUTION GRID UNDER TEST

Detection and classification analysis are carried out by using the IEEE 33-bus test feeder, which is shown in Fig. 9. All simulations are carried out in Matlab/Simulink software by employing a sampling frequency of 6.4 kHz. All fault scenarios are performed between buses 3 and 23, corresponding to the distribution line identified as L3-23. The data set includes non-fault scenarios, HIFs, and typical faults such as single-phase-to-ground, double-phase-to-ground, and three-phase-to-ground faults. The typical faults take into account different fault locations along the distribution line, several fault resistance, and different fault inception angles; different contact surfaces for HIFs are analysed considering variations in the electric arc's conductance. Moreover, a capacitor bank switching is simulated at bus 24, load changes of linear load are assessed at bus 25, and finally, a non-linear load is modelled at bus 29.

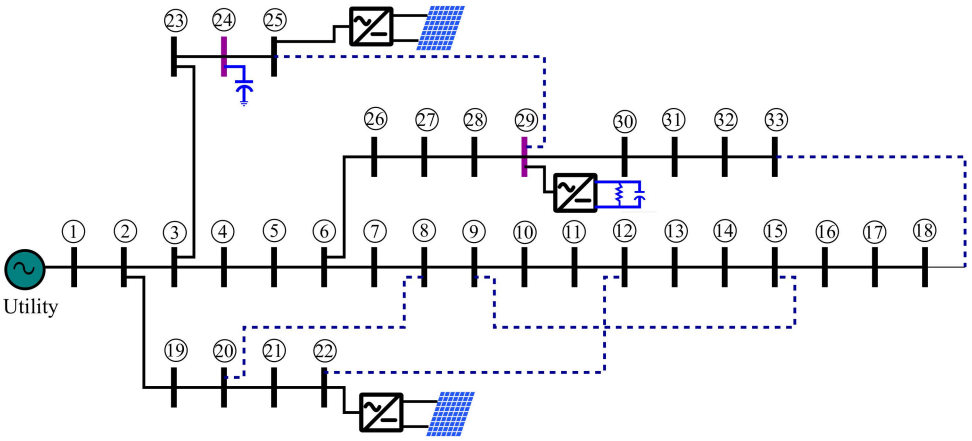


**FIGURE 9.** Modified IEEE 33-bus test feeder.

### B. DETECTION BASED ON THE HT COEFFICIENTS

HIF detection is based a sliding window analysis. In this case, the detection index is defined by the extracted features as follows:

$$\lambda(k) = N \times \left( \frac{F_1(k) + F_2(k) + F_3(k)}{3} \right) \times F_4(k) \quad (16)$$

Detection performance was studied under several fault scenarios using the test system shown in Fig. 9. For example, a HIF is simulated taking into account a power electronic converter-based distributed generator (250 kW Photovoltaic system) at bus 25. In this case, a HIF was simulated at $t = 0.5$ s and its results are depicted in Fig. 10. From Fig. 10a), it can be noticed that the line currents in the *abc* reference frame show small changes in magnitude during the fault which was simulated at $t = 0.5$s. On the other hand, Fig. b) shows the most relevant transient information during the pre-fault, fault and post-fault periods. Notice that the proposed approach can disclose the underlying high-frequency components of the analysed signal, which can be verified in Fig. 10b). After processing the HIF signal information, Fig. 10c) displays the results of the HIF detection according to the transient components-based algorithm.

To highlight the advantages of the proposed approach, a single-phase fault was simulated and its results are shown in Fig. 11. In this case, the fault was simulated at $t = 0.5$ s and the line currents observed by the protection devices are depicted in Fig. 11a). After processing the line currents, the most essential transient components are captured, and are used to extract the signal features that help identifying HIFs. These components for each line current are displayed in Fig. 11b) and the HIF detection is depicted in Fig. 11c). Therefore, in order to confirm that a HIF occurred when a transient event is detected and to avoid false classification results, it is required at least one cycle of the fundamental frequency.

Capacitor switching may be one cause of false detection as well as load changes. Therefore, the proposed approach is examined considering the transient behaviour under non-fault

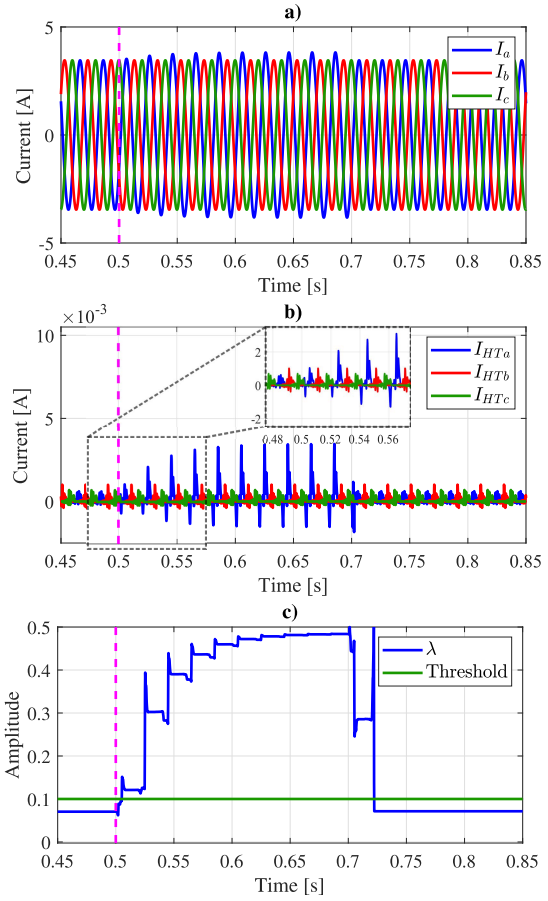


**FIGURE 10.** HIF with distributed generation: a) line currents and b) HT coefficients, and c) HIF detection using transient components-based algorithm.

conditions. For instance, Fig. 12 shows the response when a capacitor bank is energized at bus 24 (1.5 MVar). These results correspond to an energization when the voltage (Phase A as a reference) exceeds its maximum value, $t = 5.05$ s. The line currents in the *abc* reference frame are shown in Fig. 12a) and Fig. 12b) presents the results of the detection index computed by employing the HT coefficients. Notice

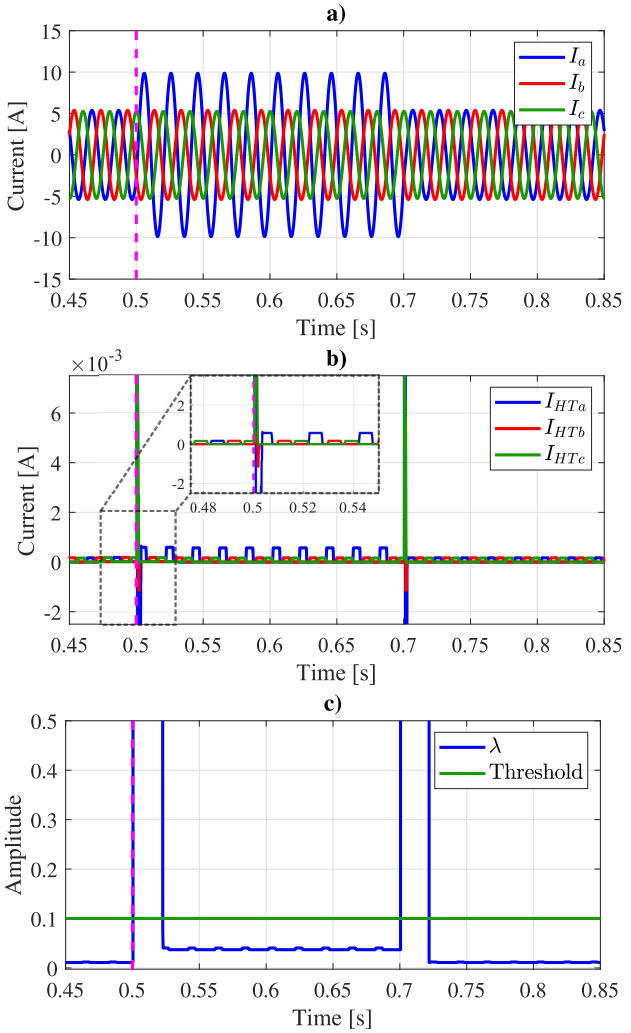


**FIGURE 11.** Single-phase fault with fault resistance of 100 Ω: a) line currents and b) HT coefficients, and c) HIF detection using transient components-based algorithm.

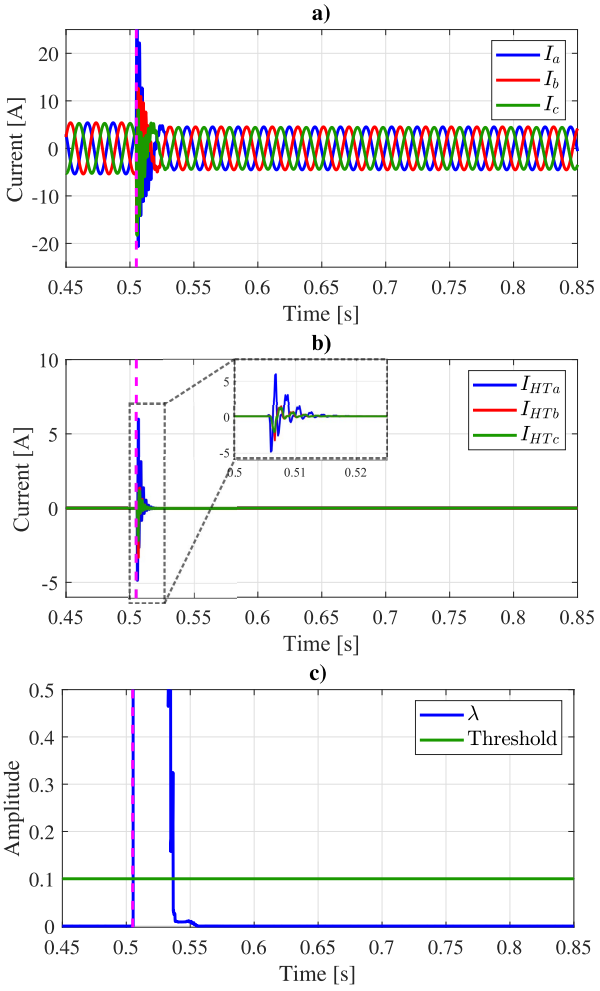


**FIGURE 12.** Capacitor switching: a) line currents and b) HT coefficients, and c) HIF detection using transient components-based algorithm.

that the transient response disappears during the first two cycles. This phenomenon may generate false classification results during the transient period, meaning that after two cycles the transient components-based algorithm will offer good performance during the detection and classification of HIFs. To ensure the detection of HIFs, it is important to remark that the transient components caused by HIFs need to persist for a long time in comparison to a transient period of a capacitor switching (or any other transient phenomenon), because this is the main information used by the proposed approach. Therefore, the protective devices must include a digital logic to avoid false operations. In this case, a delay of 2 cycles should be included in the digital logic to confirm that a HIF occurred, while other works report times between 1 and 5 cycles of the fundamental frequency [33].

Figure 13 shows the results during load changes. The change is simulated at bus 29 caused by a non-linear load. The non-linear load is energized at $t = 0.5$ s and its results are displayed in Fig. 13. In this case, a small change is taken into account, and the line currents seen by the digital protection device are shown in Fig. 13a). The corresponding transient information is captured in the HT coefficients as depicted in Fig. 13b). Notice that the load change presents significant differences along time as shown in Fig. 13c), nevertheless, this event is correctly identified as a non-faulted condition.

Based on these results, the proposed method exhibits good performance detecting faults. Detection time depends on the sampling frequency. In this case, the average time is 20.2 ms, with a system frequency of 50 Hz. Before the average time, a HIF can not be correctly detected and may be classified as a non-fault condition. In consequence, the performance of the classifiers may also be affected. Therefore, to improve the detection and classification of HIFs, this approach needs at least two cycles of the fundamental frequency. Higher accuracy and reliability entail a longer detection time. In the case of HIFs accuracy is important to avoid additional problems based on the complex nature of the electric arc phenomenon.

### C. CLASSIFICATION RESULTS

Table 1 depicts the results reached by the classification process. Based on these results, KNN presented better

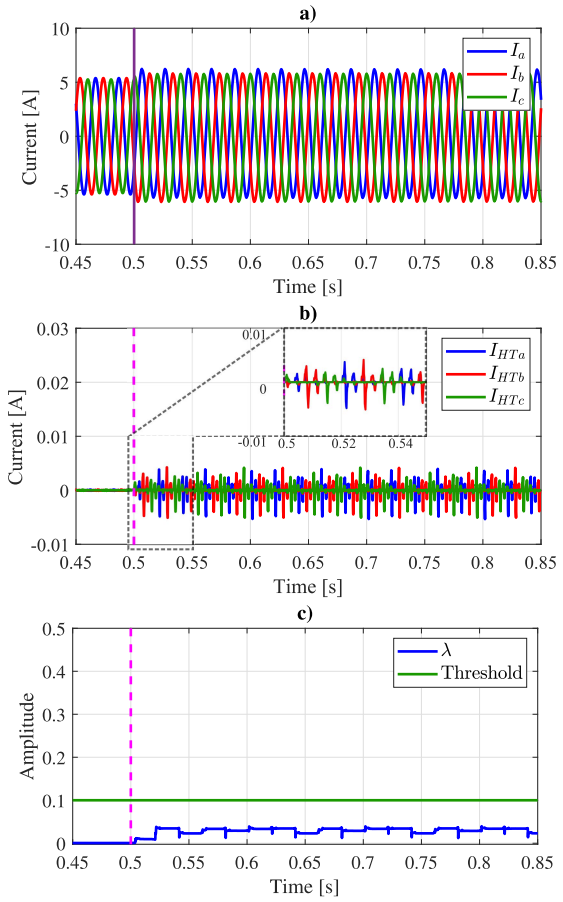


**FIGURE 13.** Load change at bus 29: a) line currents and b) HT coefficients, and c) HIF detection using transient components-based algorithm.

**TABLE 1.** Proposed approach using HT and DWT.

| Classifier | Accuracy (%) | |
|---|---|---|
| | DWT | HT |
| SVM | 94.7122 | 98.1538 |
| KNN | 98.8191 | 99.2722 |
| ANN | 84.7286 | 92.0189 |

performance than SVM and ANN. In addition, for comparison purposes the studied faults were also processed by the discrete wavelet transform (DWT) using 6 decomposition levels with the mother wavelet Daubechies 4 (Db4). In this case, a set of features was defined in a similar way to the HT, namely, statistical moments obtained from the wavelet high frequency bands at different resolution levels.

Results show that both signal processing techniques present small differences when the KNN classifier is applied, and the most significant discrepancy appears with the other two classifiers. Fig. 14 presents the confusion matrix for the proposed approach using the KNN classifier. Notice in Fig. 14, that the false-positives of the HIFs are identified as non-fault conditions.

Another topic to analyse is the classification metrics and their behaviour when an unbalanced data set is employed. For example, in this application, a critical condition occurs when the protection systems are not capable of detecting


**FIGURE 14.** Confusion matrix using HT and KNN classifier with a balanced data set.

**TABLE 2.** Proposed approach using an unbalanced data set.

| Classifier | Accuracy (%) | |
|---|---|---|
| | DWT | HT |
| SVM | 96.3636 | 97.5152 |
| KNN | 98.8182 | 98.7273 |
| ANN | 96.9697 | 96.9697 |

any condition of HIFs, that is, the fault could be classified as a non-fault scenario. This represents a critical scenario compared to misclassification resulting in other fault types, for example, a double-phase fault which is identified as a three-phase fault. In this sense, an unbalanced data set was employed to assess the proposed method whose results are shown in Table 2 and Fig. 15. It can be noticed that the results present significant changes in the classifiers as shown in Table 2. However, the best results still correspond to the KNN classifier while the ANN improves in comparison with the results shown in Table 1. Moreover, the SVM offers small changes in both scenarios, balanced and unbalanced data set.

Finally, the confusion matrix obtained is depicted in Fig. 15. Notice that HIFs produce false positives identified as non-fault events and double-phase faults. A HIF classified as a fault (no matter which fault type), is preferred over a HIF identified as a non-fault event. Finally, the comparison results after applying the DWT show that both techniques generate similar results, and the best results are achieved by the KNN classifier. In terms of complexity both DWT and HT demand a similar computational burden. The advantage of the HT relies on the basis functions that are better suited to detect signal changes in time-frequency since they consist of Gaussian derivatives of different orders at different scales, whereas the DWT has a single basis function (mother wavelet) at different scales. In conclusion, the proposed method presents better performance for the discussed scenarios.

For comparison purposes, other methods reported in the literature were analysed to validate the effectiveness of the proposed method. Table 3 shows the results obtained using different methods. For example, the DWT-based algorithm reported in [13] considers five decomposition levels and employs only two features such as energy and standard deviation whose accuracy was 98.3298 %. In [21] a classification

**TABLE 3.** HIF classification comparison results using other approaches.

| Method | Tool | Classifier | Accuracy (%) |
|---|---|---|---|
| [13] | DWT | KNN | 98.3298 |
| [21] | PCA | SVM | 98.8273 |
| [28] | DWT | ANN | 97.52* |
| [16] | EMD | KNN | 97.9515-98.2000* |
| [34] | STFT | CNN | 98.6700* |
| Proposed | HT | KNN | 99.2722 |


**FIGURE 15.** Confusion matrix using HT and KNN classifier with an unbalanced data set.

method based on principal component analysis (PCA) is performed, where only the most significant six features are employed for the classification process producing a effectiveness of 98.8273 %. Another similar approach is discussed in [28], where eight features are taken into consideration for the classification approach; in this case, the authors used five decomposition levels and Daubechies 5 as the mother wavelet. Empirical mode decomposition is also employed for comparison purposes [16], where features were obtained in ten resolution levels according to each intrinsic mode function; in this case, authors reported a accuracy of 98.2 %, however, we obtained 97.9515% with the data used in this research is. The Short-time Fourier transform (STFT) has also been used to detect HIF. The effectiveness of this technique was proven in [34], with a classification based on a convolutional neural network (CNN), showing an overall accuracy of 98.76 %.

## VI. CONCLUSION

A new method for fault detection and classification of HIFs in distribution systems was proposed. This approach analyses the high-frequency components of the electrical signal by means of the the Hermite Transform on a multiresolution. The method was tested under different transient scenarios, proving good performance in the discrimination of HIFs from other types of faults. In addition, the non-fault transient events were discussed to show that high-frequency components, produced by the non-linear load changes, depend on the load capacity. This means that larger load changes (non-linear load), may produce misclassification depending on the harmonic content. Based on the results, the transient components analysis method exhibited good performance and effectiveness for different analysed scenarios, thanks to the properties of the HT analysis functions. The HT coefficients play a key role extracting essential characteristic features during the transient period of electrical signals. The Hermite transform presents several advantages with respect to the DWT, due to the localization properties of the Gaussian function and its derivatives in time and frequency. They extract the most relevant transient information which was used to build statistical indexes. Finally, different classifiers such as SVM, KNN, and ANN showed good accuracy, taking as inputs the statistical indexes defined by the HT coefficients. The obtained results were compared with the DWT, and it was found that KNN offered better performance than the other classifiers in both methods.

## REFERENCES

[1] O. A. Gashteroodkhani, M. Majidi, and M. Etezadi-Amoli, "Fire hazard mitigation in distribution systems through high impedance fault detection," *Electr. Power Syst. Res.*, vol. 192, Mar. 2021, Art. no. 106928.
[2] R. B. G. Grimaldi, T. S. A. Chagas, J. Montalvão, N. S. D. Brito, W. C. dos Santos, and T. V. Ferreira, "High impedance fault detection based on linear prediction," *Electr. Power Syst. Res.*, vol. 190, Jan. 2021, Art. no. 106846.
[3] M. Biswal, S. Ghore, O. P. Malik, and R. C. Bansal, "Development of time-frequency based approach to detect high impedance fault in an inverter interfaced distribution system," *IEEE Trans. Power Del.*, vol. 36, no. 6, pp. 3825–3833, Dec. 2021.
[4] J. Tengdin, R. Westfall, and K. Stephan, "High impedance fault detection technology," IEEE Power Syst. Relaying Committee, Piscataway, NJ, USA, Rep. PSRC Work. Group D15, 1996. [Online]. Available: https://grouper.ieee.org/groups/td/dist/documents/highz.pdf
[5] V. Torres, J. L. Guardado, H. F. Ruiz, and S. Maximov, "Modeling and detection of high impedance faults," *Int. J. Electr. Power Energy Syst.*, vol. 61, pp. 163–172, Oct. 2014.
[6] S. Chakraborty and S. Das, "Application of smart meters in high impedance fault detection on distribution systems," *IEEE Trans. Smart Grid*, vol. 10, no. 3, pp. 3465–3473, May 2019.
[7] J. R. Macedo, J. W. Resende, C. A. Bissochi, D. Carvalho, and F. C. Castro, "Proposition of an interharmonic-based methodology for high-impedance fault detection in distribution systems," *IET Gener., Transmiss. Distrib.*, vol. 9, no. 16, pp. 2593–2601, Dec. 2015.
[8] D. A. Gadanayak and R. K. Mallick, "Interharmonics based high impedance fault detection in distribution systems using maximum overlap wavelet packet transform and a modified empirical mode decomposition," *Int. J. Elect. Power Energy Syst.*, vol. 112, pp. 282–293, Nov. 2019.
[9] F. B. Costa, B. A. Souza, N. S. D. Brito, J. A. C. B. Silva, and W. C. Santos, "Real-time detection of transients induced by high-impedance faults based on the boundary wavelet transform," *IEEE Trans. Ind. Appl.*, vol. 51, no. 6, pp. 5312–5323, Nov./Dec. 2015.
[10] F. B. Costa, "Boundary wavelet coefficients for real-time detection of transients induced by faults and power-quality disturbances," *IEEE Trans. Power Del.*, vol. 29, no. 6, pp. 2674–2687, Dec. 2014.
[11] W. C. Santos, F. V. Lopes, N. S. D. Brito, and B. D. Souza, "High-impedance fault identification on distribution networks," *IEEE Trans. Power Del.*, vol. 32, no. 1, pp. 23–32, Feb. 2017.
[12] S. Roy and S. Debnath, "PSD based high impedance fault detection and classification in distribution system," *Measurement*, vol. 169, Feb. 2021, Art. no. 108366.
[13] K. S. V. Swarna, A. Vinayagam, M. B. J. Ananth, P. V. Kumar, V. Veerasamy, and P. Radhakrishnan, "A KNN based random subspace ensemble classifier for detection and discrimination of high impedance fault in PV integrated power network," *Measurement*, vol. 187, Jan. 2022, Art. no. 110333.
[14] K. Sekar and N. K. Mohanty, "Data mining-based high impedance fault detection using mathematical morphology," *Comput. Electr. Eng.*, vol. 69, pp. 129–141, Jul. 2018.
[15] M. Kavi, Y. Mishra, and M. D. Vilathgamuwa, "High-impedance fault detection and classification in power system distribution networks using morphological fault detector algorithm," *IET Gener., Transmiss. Distrib.*, vol. 12, no. 15, pp. 3699–3710, Aug. 2018.

[16] H. Lala and S. Karmakar, "Detection and experimental validation of high impedance arc fault in distribution system using empirical mode decomposition," *IEEE Syst. J.*, vol. 14, no. 3, pp. 3494–3505, Sep. 2020.
[17] M. Sarlak and S. Shahrtash, "High impedance fault detection using combination of multi-layer perceptron neural networks based on multi-resolution morphological gradient features of current waveform," *IET Gener., Transmiss. Distrib.*, vol. 5, no. 7, pp. 588–595, 2011.
[18] J. G. S. Carvalho, A. R. Almeida, D. D. Ferreira, B. F. dos Santos, L. H. P. Vasconcelos, and D. de Oliveira Sobreira, "High-impedance fault modeling and classification in power distribution networks," *Electr. Power Syst. Res.*, vol. 204, Mar. 2022, Art. no. 107676.
[19] D. P. S. Gomes, C. Ozansoy, and A. Ulhaq, "High-sensitivity vegetation high-impedance fault detection based on signal's high-frequency contents," *IEEE Trans. Power Del.*, vol. 33, no. 3, pp. 1398–1407, Jun. 2018.
[20] A. Ghaderi, H. A. Mohammadpour, H. L. Ginn, and Y. J. Shin, "High-impedance fault detection in the distribution network using the time-frequency-based algorithm," *IEEE Trans. Power Del.*, vol. 30, no. 3, pp. 1260–1268, Jun. 2015.
[21] M. Eslami, M. Jannati, and S. S. Tabatabaei, "An improved protection strategy based on PCC-SVM algorithm for identification of high impedance arcing fault in smart microgrids in the presence of distributed generation," *Measurement*, vol. 175, Apr. 2021, Art. no. 109149.
[22] K. Sarwagya, S. De, and P. K. Nayak, "High-impedance fault detection in electrical power distribution systems using moving sum approach," *IET Sci., Meas. Technol.*, vol. 12, no. 1, pp. 1–8, Jan. 2018.
[23] L. U. Iurinic, A. R. Herrera-Orozco, and R. G. Ferraz, "Distribution systems high-impedance fault location: A parameter estimation approach," *IEEE Trans. Power Del.*, vol. 31, no. 4, pp. 1806–1814, Aug. 2016.
[24] J.-B. Martens, "The Hermite transform-theory," *IEEE Trans. Acoust., Speech Signal Process.*, vol. 38, no. 9, pp. 1595–1606, Sep. 1990.
[25] A. P. Witkin, "Scale-space filtering," in *Proc. 8th Int. Joint Conf. Artif. Intell.*, vol. 2. San Francisco, CA, USA: Morgan Kaufmann, 1983, pp. 1019–1022.
[26] J. L. Silvan-Cardenas and B. Escalante-Ramirez, "The multiscale Hermite transform for local orientation analysis," *IEEE Trans. Image Process.*, vol. 15, no. 5, pp. 1236–1253, May 2006.
[27] M. Mishra and R. R. Panigrahi, "Taxonomy of high impedance fault detection algorithm," *Measurement*, vol. 148, Dec. 2019, Art. no. 106955.
[28] V. S. B. Kurukuru, F. Blaabjerg, M. A. Khan, and A. Haque, "A novel fault classification approach for photovoltaic systems," *Energies*, vol. 13, no. 2, p. 308, Jan. 2020.
[29] S. Ahmad, N. Hasan, V. S. B. Kurukuru, M. A. Khan, and A. Haque, "Fault classification for single phase photovoltaic systems using machine learning techniques," in *Proc. 8th IEEE India Int. Conf. Power Electron. (IICPE)*, Dec. 2018, pp. 1–6.
[30] O. Yaman, "An automated faults classification method based on binary pattern and neighborhood component analysis using induction motor," *Measurement*, vol. 168, Jan. 2021, Art. no. 108323.
[31] P. Ghalyani and A. H. Mazinan, "Performance-based fault detection approach for the dew point process through a fuzzy multi-label support vector machine," *Measurement*, vol. 144, pp. 214–224, Oct. 2019.
[32] H. A. Illias, X. R. Chai, and A. H. A. Bakar, "Hybrid modified evolutionary particle swarm optimisation-time varying acceleration coefficient-artificial neural network for power transformer fault diagnosis," *Measurement*, vol. 90, pp. 94–102, Aug. 2016.
[33] M. Bhatnagar, A. Yadav, and A. Swetapadma, "A resilient protection scheme for common shunt fault and high impedance fault in distribution lines using wavelet transform," *IEEE Syst. J.*, early access, May 19, 2022, doi: 10.1109/JSYST.2022.3172982.
[34] T. Sirojan, S. Lu, B. T. Phung, D. Zhang, and E. Ambikairajah, "Sustainable deep learning at grid edge for real-time high impedance fault detection," *IEEE Trans. Sustain. Comput.*, vol. 7, no. 2, pp. 346–357, Apr. 2022.

**DANIEL GUILLEN** (Member, IEEE) received the B.Eng. degree in electrical engineering from the Instituto Tecnologico de Morelia, Mexico, in 2007, and the M.Sc. and Ph.D. degrees in electrical engineering from the Universidad Autonoma de Nuevo Leon, Mexico, in 2010 and 2015, respectively. He was with the National Center of Energy Control (CENACE-Mexico) conducting interconnection studies of renewable energy, such as solar and wind power plants, from 2015 to 2016. He was an Associate Professor with the Universidad Nacional Autonoma de Mexico, from 2016 to June 2018. He is currently with the Tecnológico de Monterrey. He is also a member of the National Research System, National Council of Science and Technology (CONACyT-Mexico), Level 1 (SNI-1). His research interests include power system modeling, power system protection, wide-area monitoring, signal processing, and transient analysis.

**JIMENA OLVERES** received the B.S. degree in biomedical engineering from the Universidad Iberoamericana in Mexico City, and the master's degree in engineering and the Ph.D. degree in computer science from the Universidad Nacional Autónoma de México (UNAM). She is currently a Professor at the UNAM. Her research interests include machine learning, computer vision, and image and signal processing.

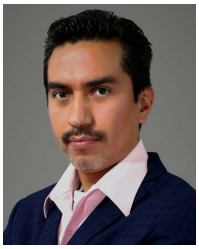

**VICENTE TORRES-GARCÍA** (Senior Member, IEEE) was born in Morelia, Michoacán, Mexico. He received the M.Sc. and Ph.D. degrees in electrical engineering from the Instituto Tecnológico de Morelia, in 2009 and 2015, respectively. He is currently an Associate Professor with the Department of Electrical Energy, Universidad Nacional Autónoma de México. His research interests include electric power systems, distribution networks, harmonics, electromagnetic transients, and power systems.

**BORIS ESCALANTE-RAMÍREZ** received the Ph.D. degree from the Technical University of Eindhoven, in 1992. He is currently a Professor at the Universidad Nacional Autónoma de México. His research interests include bioinspired models for computer vision, and image and signal processing.